AIAA JOURNAL
Vol. 32, No. 12, December 1994

Numerical Model of Boundary-Layer Control Using Air-Jet Generated Vortices

F. S. Henry* and H. H. Pearcey†
City University, London EC1V OHB, England, United Kingdom

Numerical calculations of the three-dimensional flowfield generated by pitched and skewed air jets issuing into an otherwise undisturbed turbulent boundary layer are presented. It is demonstrated that each such jet produces a single strong longitudinal vortex. The strength of the vortex, as inferred from its effect on the development of skin friction, is shown to be influenced by pitch and skew angles, exit velocity, and downstream distance in ways which accord with published experimental results. The calculated beneficial effect that the longitudinal vortices have on the development of skin friction in an adverse pressure gradient demonstrates the mechanism by which vortex generators delay boundary-layer separation. It follows that the numerical model could be used to optimize arrays of air-jet vortex generators. Furthermore, the facility to quantify the interaction between the vortex and the boundary layer should also be valuable in the application of vane vortex generators, and possibly even more generally.

Nomenclature

A = slot aspect ratio
C = constant, see Eq. (11)
C_f = coefficient of skin friction, $2\tau_w/\rho U_0^2$
D = solution domain width
D_h = jet slot hydraulic diameter
d = slot length
F = h/δ
h = local solution domain height
k = turbulence kinetic energy
k_{jet} = turbulence kinetic energy at jet exit plane
L = solution domain length
l = Prandtl's mixing length
P = pressure along solution domain upper boundary
$P_{\max}$ = pressure at solution domain exit
R = U_{jet}/U_0
$Re_{x'}$ = local Reynolds number, $\rho U_0 x'/\mu$
U = streamwise velocity
U_{jet} = jet flow mean velocity
U_0 = main flow mean velocity
$\overline{u'v'}$ = Reynolds stress
u_τ = $(\tau_w/\rho)^{\frac{1}{2}}$
V = cross-stream velocity normal to plate
W = cross-stream velocity parallel to plate
w = slot width
w' = projected slot width, see Fig. 2
x = mean flow direction measured from jet slot centerline
x' = mean flow direction measured from plate's leading edge
x'' = mean flow direction measured from solution domain inlet
y = cross-stream direction normal to plate
y^+ = yu_τ/ν
z = cross-stream direction parallel to plate
δ = theoretical boundary-layer height, $0.37x'(Re_{x'})^{-1/5}$
ε = dissipation rate of turbulence energy
ε_{jet} = dissipation rate of turbulence energy at jet exit plane
θ = jet pitch angle
μ = absolute viscosity
ν = μ/ρ
ρ = density
τ_w = wall shear stress
ϕ = jet skew angle

Received Sept. 2, 1993; revision received April 16, 1994; accepted for publication June 2, 1994.

*Senior Research Fellow, Department of Mechanical Engineering and Aeronautics.

†Visiting Professor, Department of Mechanical Engineering and Aeronautics.

I. Introduction

THE principle of boundary-layer control by longitudinal vortices trailing over the surface has been used extensively to delay the separation of turbulent boundary layers ever since the introduction of vane vortex generators by Taylor[1] in 1950. The possibility of generating the vortices by inclined air jets instead of vanes was first investigated by Wallis[2] and reviewed, with further results, by Pearcey.[3] Interest has more recently been revised by further experimental studies of air-jet vortex generators and their application to suppress boundary-layer separation (see, for example, Johnston and Nishi,[4] Compton and Johnston,[5] Selby et al.,[6] and Pearcey et al.[7]). This revival has in turn triggered the quest for the means to quantify the fluid dynamic processes involved.

The purpose of this paper is to present an initial account of a numerical study of the vortex generation and the subsequent interaction between vortices and boundary layer. Specifically, the problem considered is that of an incompressible turbulent boundary layer over a flat plate into which are issuing pitched and skewed air jets. The aims of the study were: to show that it was possible to model the three-dimensional flow numerically with reasonable accuracy using comparisons with published experimental results where possible, to investigate the influence of some of the various parameters of the problem, and to quantify the manner in which the vortices sustain positive skin friction in an adverse pressure gradient that would otherwise cause the boundary layer to separate.

In the following, a brief account is given of the numerical code used to solve the governing equations. Details of the flow, solution domain, gridding, and boundary conditions are then discussed. In the remaining sections, predictions of the flowfields generated by air jets issuing into incompressible turbulent boundary layers with and without axial pressure gradients are discussed in detail. Particular emphasis is placed on how the results relate to the use of such devices to control boundary-layer separation.

The ability to quantify the interaction between the vortices and boundary layer has been conspicuous by its absence in the extensive applications of vane vortex generators, and so the model should be useful in this context also.

II. Governing Equations and Their Numerical Solution

Discrete versions of the equations governing the conservation of mass and momentum of a Newtonian fluid were solved using CFDS-FLOW3D Release 2.4,[8] which is a general purpose suite of programs for the prediction of laminar and turbulent flow and heat transfer. Whereas CFDS-FLOW3D can model both compressible

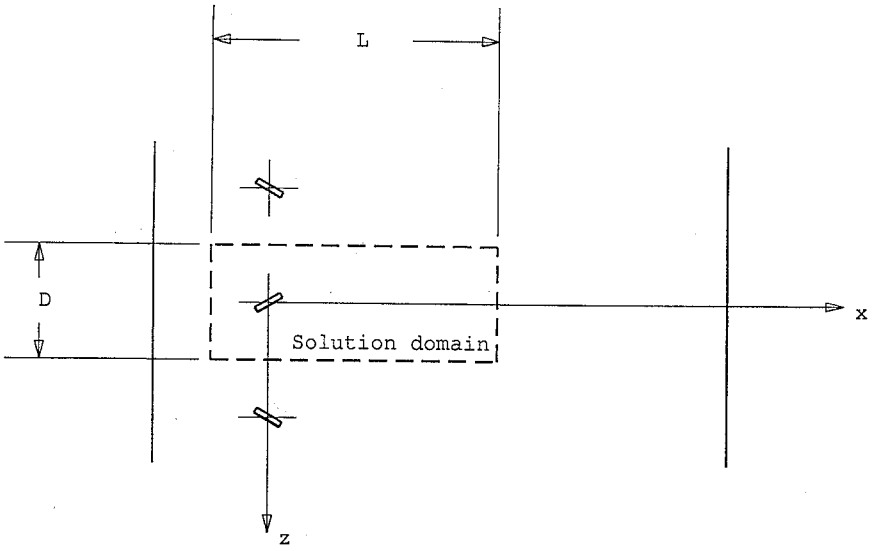

Fig. 1 Air-jet slot configuration.

and incompressible flows, the present study was restricted to the incompressible case. The code uses the finite volume method to solve the governing equations in general, nonorthogonal, body-fitted coordinates. Body-fitted coordinates were essential for the accurate gridding of the jet slot configuration used in this study.

The default turbulence model in CFDS-FLOW3D is the k-ε model, which is used in conjunction with standard wall functions. These defaults were used in the present calculations. However, it is recognized that the k-ε model and the use of wall functions have been shown to have limitations (e.g., see Henry and Reynolds[9]), particularly for the prediction of swirling flows (e.g., see Bradshaw,[10] or Henry and Collins[11]). CFDS-FLOW3D does offer more precise models of turbulence, at the expense of increased computer storage and CPU time. However, it was felt that the k-ε model was adequate for what were essentially exploratory calculations and that the more precise models could be used, if necessary, in future calculations, once the basic concepts had been demonstrated.

III. Flow and Gridding Details

A. Flow and Solution Domain

The problem considered is that of the steady flow of air over an infinitely wide, 1 m long, flat plate. Jets of air enter the main flow from rectangular slots in the plate. The Reynolds number of the main flow based on the plate length was set to 5×10^6. The density ρ and absolute viscosity μ of air were taken to be 1.21 kg/m^3 and 1.91×10^{-5} kg/ms, respectively. The mean velocity of the jet flow U_{jet} was set to a multiple R of the mean velocity of the main flow at inlet U_0. As can be seen in Fig. 1, the slots are equispaced along a line that runs parallel with the plate's leading edge. The jet slots were taken to be 0.2 m from the leading edge and spaced 0.2 m apart. It can also be seen that the slots are arranged such that the air jets enter the main flow at alternating skew angles of ϕ and $-\phi$ to the mean flow direction (the x direction). Details of the slots are given in Fig. 2, where it can be seen that the jets also enter the main flow at a pitch angle of θ to the plate. The slot aspect ratio A is defined as $A = d/w$, where w is the true slot width; i.e., not the projected width w' (unless $\theta = 90$ deg).

For the jet configuration considered, it was only necessary to model one air jet because the plane midway between each pair of jets is a plane of symmetry. Hence, the side boundaries of the solution domain were placed coincident with these symmetry planes. Thus, the solution domain width D was identical to the distance between slots, i.e., 0.2 m. The boundaries of the solution domain are depicted by a broken line in Fig. 1. As it is computationally more efficient to assume that the flow enters the solution domain with a well-defined boundary layer, the entrance plane of the solution domain was placed 0.1 m downstream of the plate's leading edge. The solution domain length L was set to 0.5 m. The top boundary of the solution domain

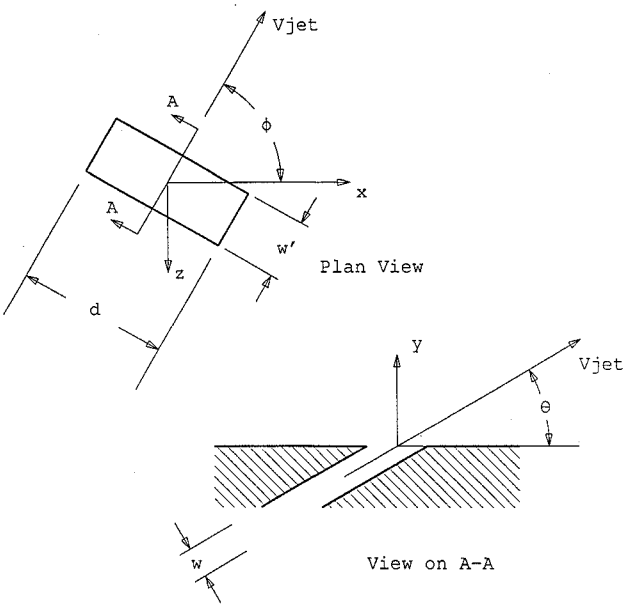

Fig. 2 Jet slot details.

was made to increases with downstream direction. The local height of the solution domain h was defined to be a multiple F of the theoretical boundary-layer height for turbulent flow δ where δ was estimated using

$$\delta = 0.37x'(Re_{x'})^{-1/5} \tag{1}$$

where $Re_{x'} = \rho U_0 x'/\mu$, and x' is measured from the plate's leading edge. In all but one of the calculations to be discussed F was set to 10.

B. Gridding

The general orientation of the slot with reference to the x axis means that it is impossible to design a Cartesian grid that would allow both the sides of the slot and those of the plate to lie along grid lines. However, CFDS-FLOW3D allows the use of general nonorthogonal grids, also known as body-fitted grids. As it is computationally more efficient to have orthogonal grids wherever possible, the nonorthogonal region of the grid was restricted to a relatively small region surrounding the slot. This nonorthogonal grid was then patched to a surrounding Cartesian grid. In the y direction, the grid spacing was made to increase smoothly away from the plate. This allowed the boundary layer to be modeled with reasonable accuracy

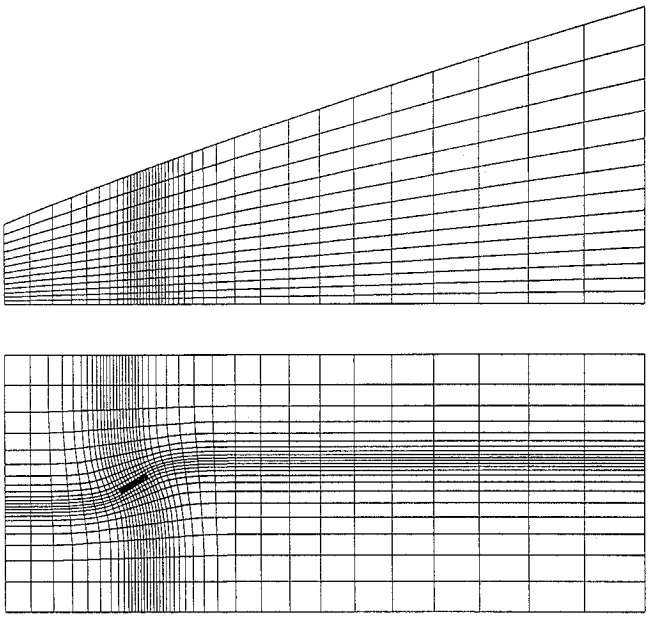

Fig. 3 Sample computational grid.

although keeping the number of control volumes to a minimum. The first increment was defined such that the centers of the control volumes coincident with the plate would be above the viscous sublayer. This is a necessary requirement of the wall treatment used in CFDS-FLOW3D for turbulent flow. Hence, assuming that the viscous sublayer height is approximately equal to $y^+ = 12$, where $y^+ = yu_\tau/\nu$, and $u_\tau = (\tau_w/\rho)^{\frac{1}{2}}$, the height of the first control volume in the y direction was set to $24\nu/u_\tau$. The wall shear τ_w was estimated using

$$2\tau_w/\rho U_0^2 = C_f = 0.059(Re_{x'})^{-1/5} \tag{2}$$

Two views of a typical grid are given in Fig. 3. Note that the grid in the y direction is shown magnified by a factor of 2, and for clarity, the first increment in the y direction was made 10 times larger that actually used in the calculations.

1. Boundary Conditions

The streamwise velocity U at inlet was assumed to be given by Prandtl's 1/7th power law i.e.,

$$U/U_0 = (y/\delta)^{1/7} \tag{3}$$

The cross-stream velocities V and W were set to zero.

The kinetic energy at inlet was estimated based on the experimental finding that the ratio of the Reynolds stress $\overline{u'v'}$ to kinetic energy is constant over most of the boundary layer. Specifically, the inlet kinetic energy was defined using

$$k = \overline{u'v'}/0.255 \tag{4}$$

The Reynolds stress was estimated using a simple eddy viscosity model, i.e.,

$$\overline{u'v'} = -l^2 \left|\frac{\partial U}{\partial y}\right| \frac{\partial U}{\partial y} \tag{5}$$

where

$$l = \kappa y \quad \text{if} \quad l < 0.085\delta$$

otherwise

$$l = 0.085\delta$$

The dissipation rate at inlet was estimated assuming local equilibrium. Hence, dissipation was equated to production of turbulence. Therefore,

$$\varepsilon = -\overline{u'v'}\frac{\partial U}{\partial y} \tag{6}$$

The velocity gradient was estimated using three-point central differencing for the internal nodes, and three-point forward and backward differencing for the first and last points, respectively. Note that, in turbulent flow calculations, CFDS-FLOW3D requires both k and ε to have positive nonzero values over the entire inlet plane. This requirement was satisfied by setting the velocity gradient to a small positive value (equal to $U_0/70\delta$) for $y > \delta$. However, in this region the velocity was set to a constant value of U_0. Flat profiles were defined for the velocity and turbulence quantities at the jet inlet. The formulas used to define the jet inlet velocity values can be written as

$$\begin{aligned} U &= U_{\text{jet}} \cos\theta \cos\phi \\ V &= U_{\text{jet}} \sin\theta \\ W &= U_{\text{jet}} \cos\theta \sin\phi \end{aligned} \tag{7}$$

where $U_{\text{jet}} = RU_0$, and values of mean kinetic energy and dissipation rate of the jet were defined using[8]

$$k_{\text{jet}} = 0.002U_{\text{jet}}^2 \tag{8}$$

and

$$\varepsilon_{\text{jet}} = \frac{k_{\text{jet}}^{3/2}}{0.3D_h} \tag{9}$$

where D_h is the hydraulic diameter of the jet slot.

The upper and exit boundaries were defined to be pressure boundaries. Unless stated otherwise, the (static) pressure on these surfaces was set to zero. It is noted that as the flow is considered incompressible, the pressure is arbitrary to an additive constant. As this constant was set to zero here, the pressure values quoted may be considered to be pressure differences from that of the undisturbed flow. For the calculations with adverse pressure gradients, the pressure distribution along the upper domain boundary was assumed to be given by

$$P = \tfrac{1}{2}P_{\max}\{\cos[\pi(x''/L - 1)] + 1\} \tag{10}$$

where x'' is measured from the solution domain inlet, and L is the length of the solution domain. As can be seen, this gives a sinusoidally varying pressure distribution with an inlet value of zero and an exit value of $P_{\max}$. Hence, in these cases, the exit plane pressure was set to $P_{\max}$.

As stated previously, the side boundaries were defined to be symmetry planes. The lower boundary was defined to be a solid surface, and boundary conditions on this surface were implemented using the standard wall-function approach.

IV. Predictions

A. General Details

Details of the 14 cases considered are given in Table 1. It is noted that the jet cross-sectional area was kept at a constant value of 1.25×10^{-4} m^2 throughout. Hence, all cases with the same jet velocity have the same mass flow rate. The last column in the table refers to the pressure at the exit plane. Cases for which $P_{\max}$ is zero represent boundary layers with zero streamwise pressure gradient, and cases for which $P_{\max}$ is nonzero represent boundary layers with adverse pressure gradients.

All calculations were performed on a Sun sparcstation 2. In most cases, reasonable convergence was achieved in 2000 iterations. For a typical grid of 31,450 ($37 \times 34 \times 25$) active control volumes, this took approximately 13 h.

Table 1 Details of cases considered

Case	Pitch angle θ, deg	Skew angle ϕ, deg	Slot aspect ratio A	Velocity ratio R	P_{max}, kPa
1	90	0	1.0	1.0	0.0
2	15	60	5.0	1.0	0.0
3	30	60	5.0	1.0	0.0
4	45	60	5.0	1.0	0.0
5	60	60	5.0	1.0	0.0
6	30	90	5.0	1.0	0.0
7	30	45	5.0	1.0	0.0
8	30	30	5.0	1.0	0.0
9	30	60	5.0	0.5	0.0
10	30	60	5.0	2.0	0.0
11	30	60	2.5	1.0	0.0
12	30	60	1.0	1.0	0.0
13	30	60	5.0	0.0	2.7
14	30	60	5.0	2.0	2.7

B. Boundary Layers with Zero Streamwise Pressure Gradients

A plot of secondary, or cross-stream, velocity vectors downstream of a normal jet, case 1 (pitch angle $\theta = 90$ deg and skew angle $\phi = 0$ deg), is given in Fig. 4a. This case is atypical in that two, counter-rotating vortices are formed, one on either side of the jet. For all values of ϕ other than zero, only one vortex is formed. An example of the more typical structure can be seen in the cross-stream velocity vector plot for case 3 ($\theta = 30$ deg and $\phi = 60$ deg) given in Fig. 4b. Both plots represent the conditions 0.3 m downstream of the jet slot centerline. Although both jets have the same mass flow rate, it is evident that the single vortex of the skewed and pitched jet is much stronger than the two produced by the normal jet. Case 1 was included mainly to illustrate that CFDS-FLOW3D can model the general features of the classic case of a jet in cross flow, and that the single vortex seen in all other calculations was not simply an artifact of the numerical procedure employed.

It is noted that the plots in Fig. 4, and all subsequent plots, are drawn such that the viewer is looking upstream, toward the jet. Also, all velocity vector plots to be discussed were drawn to the same scale. As an indication of the scale of the cross flow relative to the that in the streamwise direction, the maximum velocity in the plot of Fig. 4b is approximately equal to $0.15U_0$.

Inspection of Fig. 4b reveals that the core of the single vortex is just above the undisturbed boundary layer, whereas the cores of the two vortices of Fig. 4a are approximately 2δ above the surface. The value of δ at this location ($x = 0.3$ m) is approximately 9.72 mm. In both cases, it was found that the vortices remain at roughly the same relative position above the surface with respect to the boundary layer.

The plots of Fig. 4 were produced using Jasper,[12] which is a software package for the postprocessing of CFDS-FLOW3D output. It is noted that the vector plots can give a false impression of the accuracy of the solution in terms of the number of points plotted. Jasper allows the user to define any number of equispaced points in each direction of the plane. The velocities at each plotted point are then interpolated from the values at grid node points. For instance, the plots of Fig. 4 have 40 points in the y direction. However, the computational grid had only 34 active control volumes, of increasing size, in this direction.

Curves of the cross-stream variation of the coefficient of skin friction $C_f = 2\tau_w/\rho U_0^2$ at a downstream location of $x = 0.3$ m for cases 1 and 3 are given in Fig. 5. Note that τ_w is the wall shear stress in the streamwise direction only. Included for comparison is the analytical curve given by Eq. (2). It is evident that the skewed and pitched jet has a larger influence on the resulting wall shear stress than does the normal jet. It is noted that CFDS-FLOW3D is able to match the analytical value of C_f in the undisturbed region of the flow. Also included are two additional predictions for case 3: one using a grid with 50% more control volumes and one with a 50% larger solution domain height (i.e., $F = 15$). It can be seen that neither refinement has a significant influence on the resulting skin friction distribution.

The influence of the pitch angle θ, skew angle ϕ, and velocity ratio, R on the wall shear stress distribution downstream of the jet is

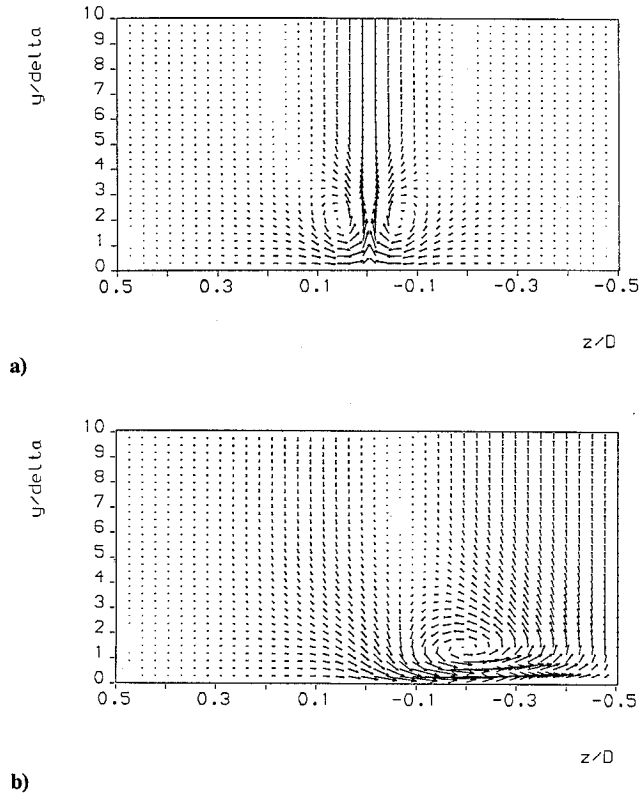

Fig. 4 Cross-stream velocity vectors, $x = 0.3$ m from jet slot centerline: a) case 1 and b) case 3.

shown in Figs. 6, 7, and 8, respectively. All three figures represent the lateral variation of skin friction coefficient 0.3 m downstream of the slot centerline. Following Johnston and Nishi,[4] the distribution of wall shear is used as a indicator of the beneficial effect, or otherwise, of the air-jet vortex generators. That is, noting the inverse relationship between boundary-layer thickness and wall shear stress and that separation occurs when the wall shear stress goes to zero, a favorable effect is deemed to be an increase of C_f above the undisturbed value.

It can be seen in Fig. 6 that the effect of decreasing the pitch angle is to increase the width of the region of the C_f curve that is above the undisturbed value. This is consistent with the experimental finding of Pearcey et al.[7] that a pitch angle of 30 deg gave a more effective result than an angle of 45 deg. The effect of varying the skew angle ϕ is shown in Fig. 7. The curves in this figure lend support to the experimental finding of Pearcey et al.[7] and the numerical results of Zhang[13] that $\phi = 60$ deg is probably optimum. It is noted that Compton and Johnston[5] concluded that the optimum value of ϕ was between 45 deg and 90 deg.

The region of increased C_f is seen in Fig. 8 to be strongly affected by the value of jet mean velocity relative to the main flow mean velocity. Conversely, it was found (data not shown) that the lateral variation of C_f is little affected by a change in slot geometry, provided the mass flow rate is kept constant. These results are consistent with the findings of Pearcey et al.[7] that exit mass flow rate had a strong influence on the control of shock-induced boundary-layer separation and that it tended to be the dominant parameter when slot size was varied. However, in the context of the predictions, it is recognized that the specification of flat profiles for all variables at the jet slot exit plane is a crude approximation to the conditions that must prevail there in reality. Kim and Benson[14] have recently demonstrated the importance of an accurate representation of the near field in establishing the flow downstream. It is further recognized that in the near-field region of the case with a jet velocity ratio of 2, the effect of compressibility may not be insignificant.

The streamwise development of the wall shear stress for a typical case (case 3) is indicated by the curves of cross-stream variation of C_f at three different downstream locations given in Fig. 9. These

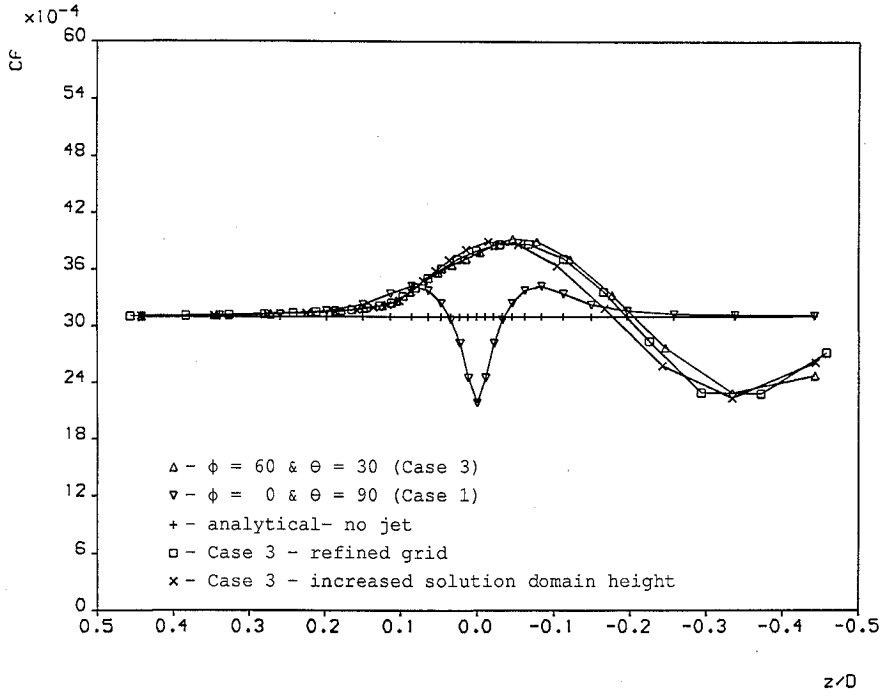

Fig. 5 Cross-stream variation of friction coefficient: comparison of normal jet and skewed and pitched jet, x = 0.3 m from jet slot centerline.

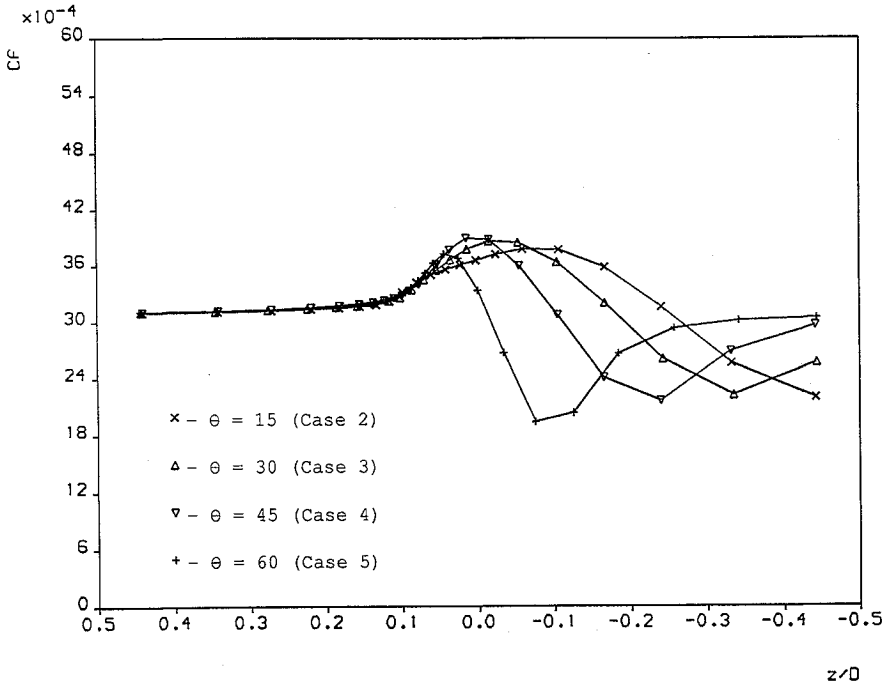

Fig. 6 Cross-stream variation of friction coefficient: effect of pitch angle θ, x = 0.3 m from jet slot centerline.

curves suggest that the vortex is moving to the left as it travels downstream. The curves also suggest the vortex becomes more diffuse and/or moves farther away from the surface as it travels downstream. The reader is reminded that the curves of C_f and the velocity vectors are drawn looking upstream, toward the jet. It will be shown in Sect. V that the lateral translation of the vortices is consistent with that calculated by the method of Jones[15] and described by Pearcey[3] for inviscid motion of a vortex in an array of counter-rotating vortices, taking into account the induced velocities of all of the vortices and their images in the wall.

C. Boundary Layers with Adverse Pressure Gradients

The ultimate aim of this work is to quantify the effects of the longitudinal vortices in delaying separation. Toward this aim, calculations of air jets in boundary layers with adverse pressure gradients were performed. Given in Fig. 10 are curves of the cross-stream variation of C_f for the case without and with a jet (cases 13 and 14) at downstream locations of $x = 0.1$ m and 0.3 m. The streamwise variation of pressure, above the boundary layer, was given by Eq. (10). The exit pressure P_{max} was adjusted until the boundary layer, without the jet, was about to separate at the exit plane; this was found to occur at $P_{max} = 2.7$ kPa. For comparison, curves for case 10 have been included. Case 10 is identical to case 14 except the former has a zero streamwise pressure gradient. These curves show clearly that the relative enhancement of C_f is actually better in an adverse pressure gradient. That is, it appears that as the boundary layer approaches separation, the width of the region which is favorably affected by the vortex increases. Hence, the vortex appears to produce the most

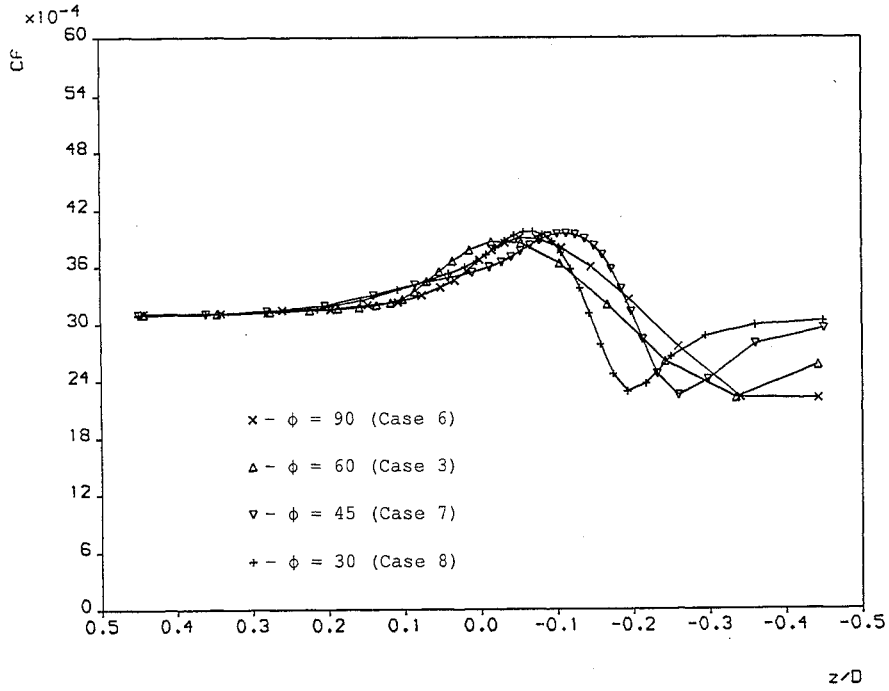

Fig. 7 Cross-stream variation of friction coefficient: effect of skew angle ϕ, x = 0.3 m from jet slot centerline.

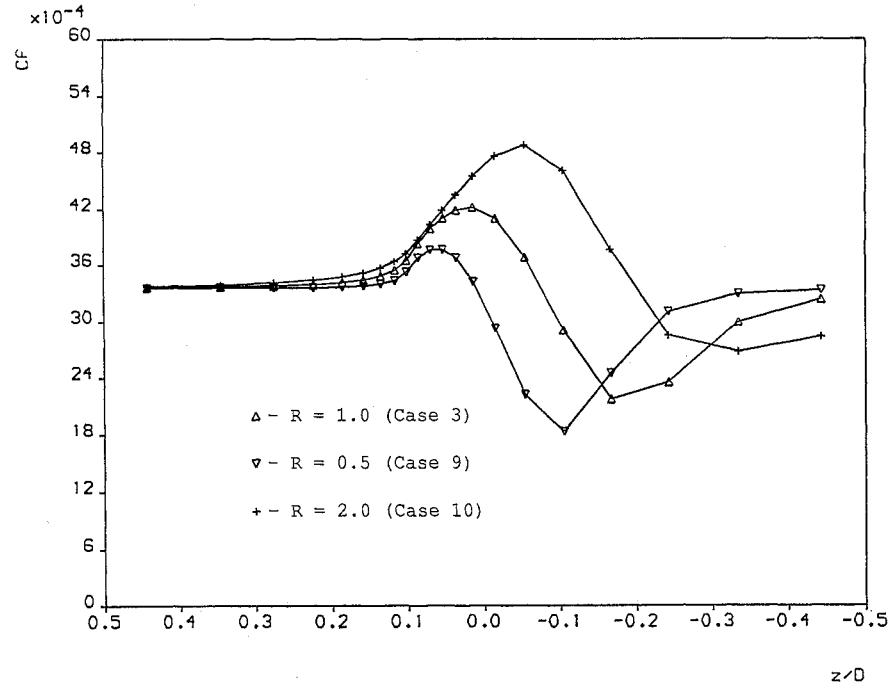

Fig. 8 Cross-stream variation of friction coefficient: effect of velocity ratio R, x = 0.3 m from jet slot centerline.

beneficial effect precisely where it is needed most. It is noted that the slight depression seen in the curve for the prediction without the jet is due to the presence of the jet slot. That is, the jet flow was switched off, but the slot was retained. The result was a local reduction in the resistance to flow.

D. Experimental Verification

Compton and Johnston[5] presented results of an experimental study of longitudinal vortices produced by pitched and skewed air jets in a turbulent boundary layer, and Compton and Johnston[16] kindly provided some of the original data from their experiments for use in this verification study. The experimental setup comprised a single round jet of 6.35 mm diameter located on the centerline of the lower wall of a rectangular constant area wind tunnel. The jet had a pitch angle equal to 45 deg. The working section of the tunnel was 13 cm high, 61 cm wide, and 200 cm long.

As it was not possible to model a round jet with the present grid without significant modification, a square jet with an equivalent cross-sectional area was used in the predictions. Also, the solution domain and grid were kept, as much as possible, equivalent to that described previously. Specifically, the sides of the solution domain were assumed to be symmetry surfaces and, hence, the numerical model assumed that there was an equispaced array of jets. Also, although in the experiment there must have been some small favorable pressure drop in the axial direction, the upper boundary was set to be a zero pressure surface. Further, the domain height was de-

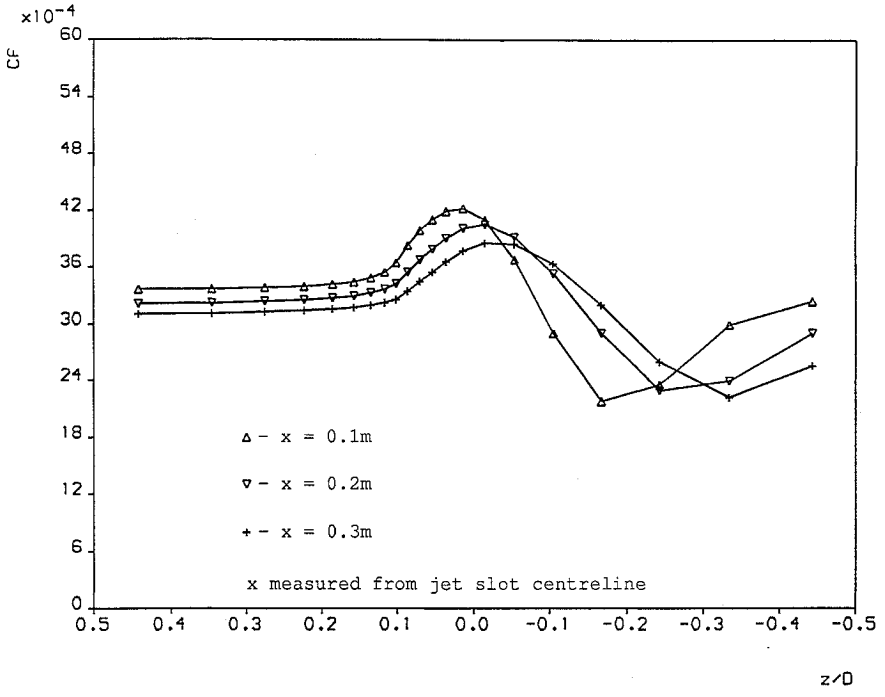

Fig. 9 Cross-stream variation of friction coefficient: downstream development, case 3.

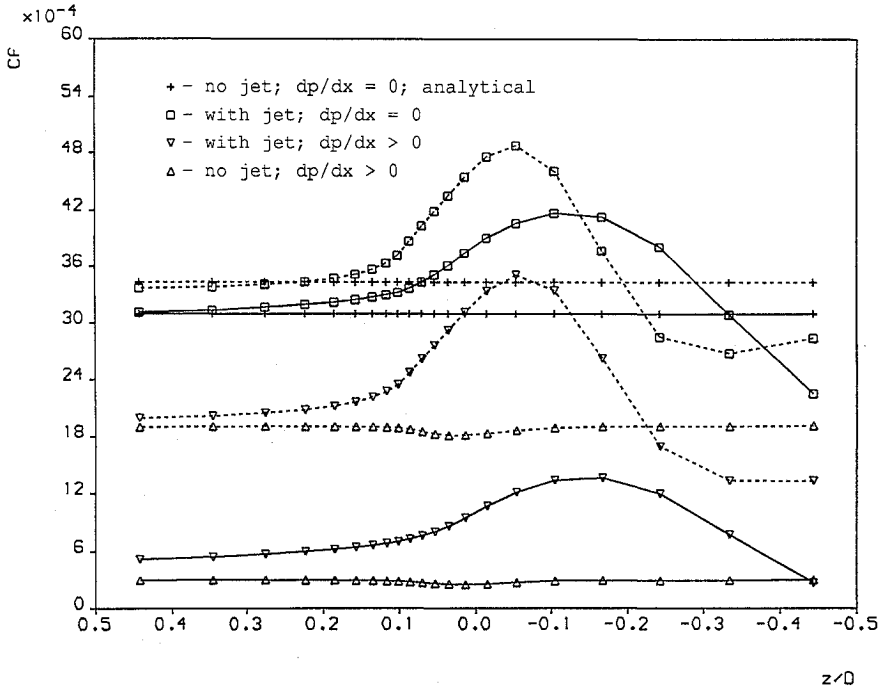

Fig. 10 Cross-stream variation of friction coefficient in adverse pressure gradient with broken line: x = 0.1 m from jet slot centerline and solid line: x = 0.3 m from jet slot centerline.

fined to increase with downstream distance as $10 \times \delta$. This implied a tunnel height considerably larger than that of the experimental tunnel.

The experiment data did not include values of skin friction, and the decay of maximum secondary-flow vorticity was chosen as the verification parameter. Given in Fig. 11 are predictions and experimental data of maximum vorticity for jets with skew angles of 0 and 90 deg for a velocity ratio of unity, and given in Fig. 12 is a comparison of predicted and experimental maximum vorticity as a function of jet velocity ratio. The mean freestream velocity was 15 m/s. Inspection of the curves in both figures reveals that although the numerical model does not always match the individual data points accurately, it is able to predict the correct trends.

V. Discussion of Results

The objective of this section is to discuss the present results in the context of what are known to be successful arrays of vane vortex generators and to use the discussion to illustrate the potential of the numerical model for quantifying the influence of the many design parameters.

A. Crossflow Patterns for Effective Mixing

The pitot pressure contours reproduced in Fig. 13 from Pearcey[3] represent a typical successful, initially equispaced, array of counter-rotating vortices produced by vanes. In particular, it is noteworthy that between adjacent pairs of downward mixing vortices (i.e., the

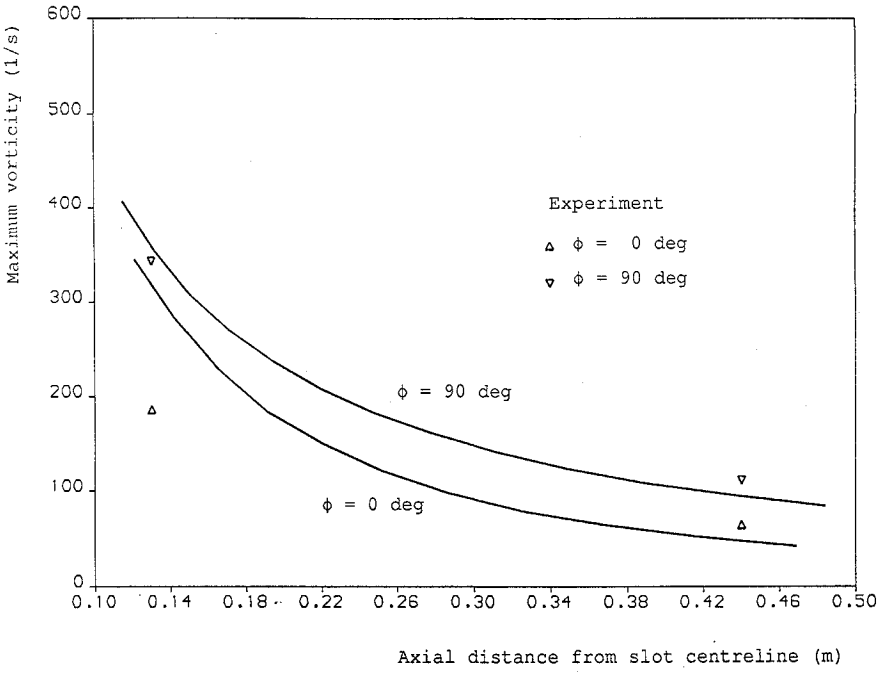

Fig. 11 Prediction of downstream decay of maximum vorticity compared with experimental data due to Compton and Johnston.[16]

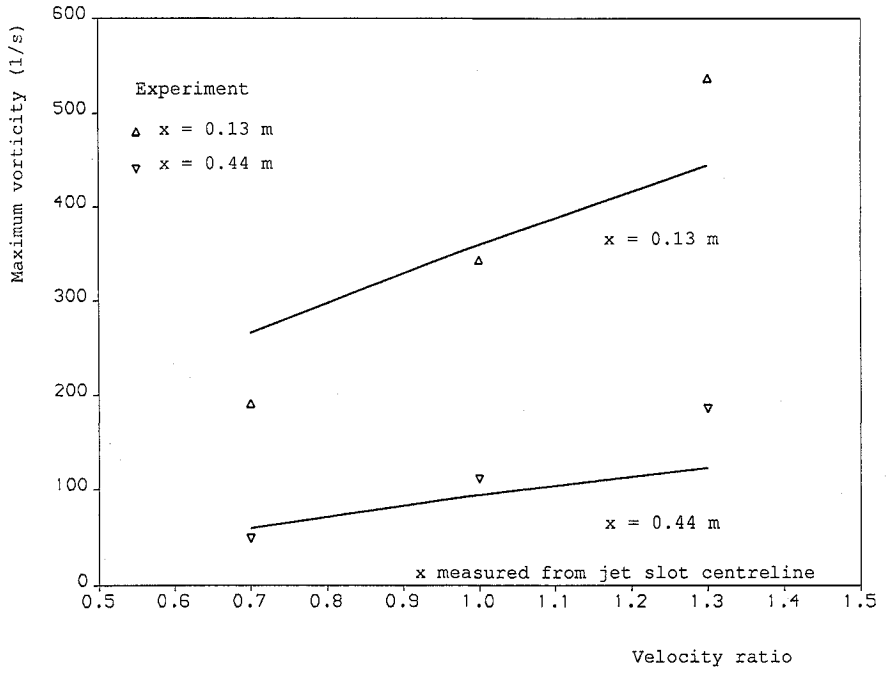

Fig. 12 Prediction of maximum vorticity with velocity ratio compared with experimental data due to Compton and Johnston.[16]

pairs between which the induced velocities are toward the surface) there is a continuous region of high skin friction (thin boundary layer) linking the respective influences of the two vortices. Similarly, the regions of low skin friction link up on the upward mixing sides of the alternate pairs.

The corresponding regions of relatively high and low skin friction are present for the current calculations (see, for example, the curves of Fig. 9). However, in this case the high and low regions do not link with the corresponding ones from the adjacent vortices on either side. This is particularly true of the downward mixing side, the left half, of the curves in Fig. 9. Such linking could no doubt readily be achieved by reducing the spacing between adjacent jets from the arbitrary spacing chosen for these initial calculations; more effective boundary-layer control should result. There is also the possibility of changing the relative spacing between pairs of downward mixing and pairs of upward mixing vortices, i.e., grouping the jet slots in pairs of opposite skew angle, but the effect of this needs to be considered in relation to that of vortex paths discussed subsequently.

B. Vortex Paths

A major consideration in choosing successful arrays of counter-rotating vortex generators, as distinct from corotating ones, are the paths adopted by the vortex pairs as they trail downstream over the surface. (The reader is directed to Pearcey[3] for a discussion of the relative merits of corotating counter-rotating vortices.) The manner in which these paths depart from the streamlines of undisturbed flow is determined by the crossflow velocities induced at the individual vortex cores by the whole array of vortices and their images in the surface. This has been analyzed by Jones[15] using inviscid, two-dimensional, or strip, theory. In particular, the pro-

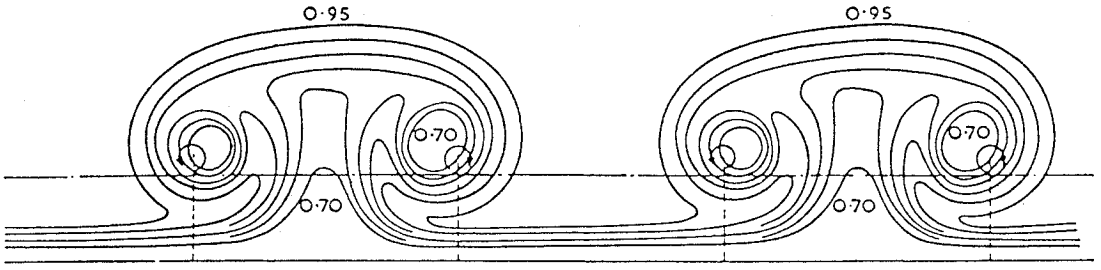

Fig. 13 Typical pitot pressure contours downstream of vane vortex generators.

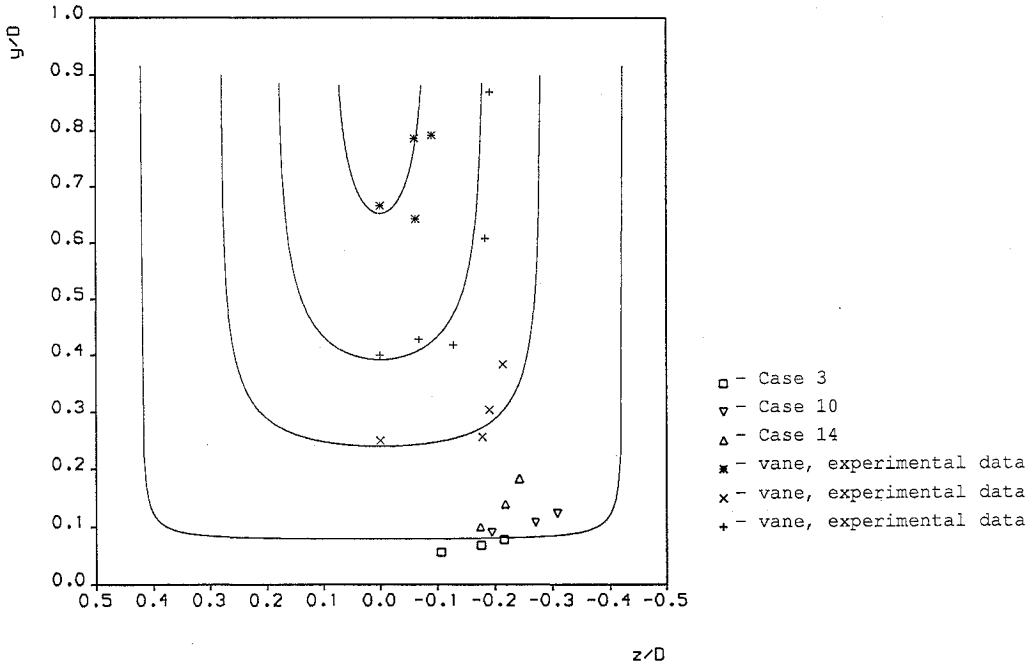

Fig. 14 Analytical, experimental, and predicted vortex paths, analytical curves given by Eq. (11).

jection of an individual vortex path in the crossflow plane is given by

$$\text{cosech}^2(\pi y/D) + \text{cosec}^2[\pi(0.5 - z/D)] = C \qquad (11)$$

where D is the distance between vanes or jet slots (also the solution domain width) and C is a constant dependent on the initial position.

Sample vortex paths, computed using Eq. (11), are given in Fig. 14. These curves represent paths taken by vortices with anticlockwise rotation viewed from downstream (as in Fig. 4). The vortices move along these paths from left to right. (Each path has images about the vertical axes at $z/D = \pm 0.5$.) Thus, if a vortex were to start well to the left on one of these projected paths, its translation will initially be toward the surface under the dominant influence of its neighboring downward mixing vortex. As it travels along its projected path, or if its origin is farther to the right, the dominant influence switches to that of the image in the surface; the translation then becomes sideways toward the neighboring upward mixing vortex on the right. Ultimately, and inexorably, the influence of this neighbor will dominate, and the vortices will move away from the surface in pairs to become ineffective for boundary-layer control. Each projected path is a characteristic locus for any origin on that locus. The projected path itself is independent of vortex strength, but the rate at which it is traced out with respect to distance over the surface is directly proportional to the vortex strength (see, for example, Robertson[17]).

The essence of choosing an array of counter-rotating vortex generators that will be effective for a given application becomes that of chosing a combination of initial height, spacing, and strength that will ensure that the vortex remains close to the surface over the required streamwise distance and at the same time will retain the spacing in pairs that gives an effective relative distribution of high to low skin friction (see preceding discussion of Fig. 13).

Each vortex path given in Fig. 14 was computed by adjusting the value of C in Eq. (11) until it represented a reasonable fit to a particular set of data. The symbols included in Fig. 14 indicate the positions of vortex centers, derived from experiments in the case of vanes or from the present calculations for air jets. As has been previously discussed by Pearcey,[3] the three lines passing through the experimental data for vane vortex generators indicate that Eq. (11) represents well the paths taken by vortices produced by vanes. The curve passing through the numerical data was chosen to best fit cases 3 and 10. It is clear that, for the air-jet configurations used here, the vortices are initially much nearer the surface than were those for the original and typical vanes; they also remain close to the surface. The contrast serves to underline the very wide range of design choice.

The paths indicated by the symbols for the two cases of vortices in zero streamwise pressure gradients (cases 3 and 10) conform approximately to the appropriate theoretical curve. The vortices are formed farther away from the surface for the greater exit velocity and trace out their characteristic cross-plane path more rapidly with respect to downstream distance. The induced cross-plane velocity of the vortex is inversely proportional to its distance from the wall and directly proportional to its strength; however, in this case, vortex strength appears to dominate.

By contrast with the cases for zero pressure gradient, the results for vortices in an adverse pressure gradient show a significantly greater movement away from the surface; this trend is presumably introduced as the mean flow is deflected away from the surface in the rapidly thickening boundary layer and is then augmented as the relative influences of neighboring and image vortices change.

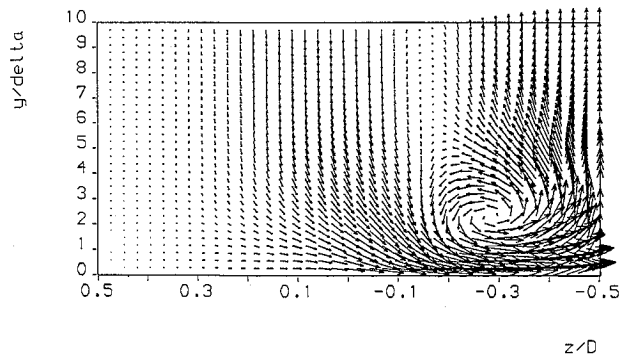

a)

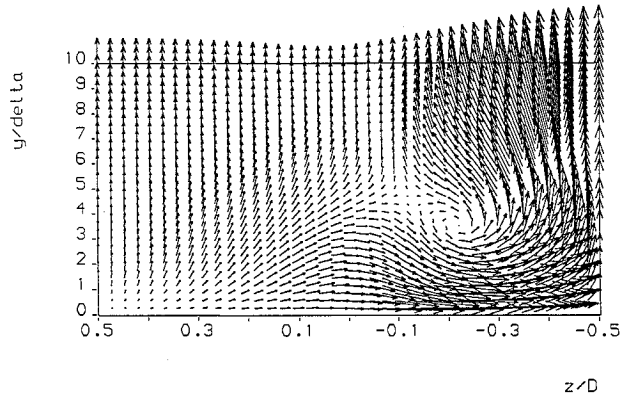

b)

Fig. 15 Cross-stream velocity vectors, x = 0.3 m from jet slot centerline: a) case 10 and b) case 14.

The two predicted paths for vortices in zero pressure gradients also move away from the surface faster than would be expected from the (inviscid) analytical solution. It is likely that this discrepancy is also due to boundary-layer thickening.

Cross-stream velocity vector plots for cases 10 and 14 are given for a downstream location of $x = 0.3$ m in Fig. 15. It was from these plots, the plots of Fig. 4 and others not presented, that the locations of the vortex centers were estimated. It is noted that these plots are drawn to the same scale as those in Fig. 4. The only difference between the vortex in Fig. 4b and that of Fig. 15a is that the latter was produced by a jet with a mass flow rate twice that of the former. Not surprisingly, it can be seen that a more energetic jet produces a stronger vortex, which results in a larger induced lateral velocity. However, the more energetic jet would appear to be able to penetrate farther into the main flow, and the resulting vortex is situated farther from the surface. As explained earlier, this should retard the lateral movement relative to a vortex (of the same strength) nearer the surface; however, it appears that vortex strength dominates in this case.

The vector plots of Fig. 15b are noticeably different from those of Fig. 15a; however, the former are consistent with expectations in that they can be viewed as the result of a superposition of the velocity field produced by the vortex and that of the crossflow, normal to the plate, of a rapidly thickening boundary layer. The differences in these plots underline the fact that the streamwise pressure gradient is an important parameter influencing the performance of these vortices as boundary-layer control devices.

It is clear from these initial examples that the optimization of vortex paths for counter-rotation vortices and hence air-jet arrays depends in a complex and interactive way on a number of variables. It is also clear, however, that just because of this, the computational model used here has significant potential for identifying the relevant parameters and for quantifying their respective influences as a basis for the optimization. There is also the prospect of improving the understanding of the respective roles of air-jet vortex generators, vane vortex generators, and the fascinating sub-boundary layer vortex generator recently used by Gulfstream (see Holmes et al.[18]).

Prospects seem to be emerging at last for developing a quantified basis for design guidelines that have so conspicuously been absent hitherto. Clearly much remains to be done in using the present model parametrically, in validating it against experiment, and, maybe, in adapting the empirical input, e.g., the turbulence modeling, if these prove to be significant.

VI. Conclusions

Boundary-layer flows over flat plates into which are issuing pitched and skewed jets have been solved numerically using CFDS-FLOW3D. The longitudinal vortices produced by these jets have been shown clearly in cross-stream velocity vector plots. Plots of the variation of the coefficient of skin friction in the cross-stream directions have been used to demonstrate the effects of changing various parameters of the problem, and the results discussed in the context of air-jet vortex generators.

Analysis of the predictions suggests that a jet with a pitch angle of 30 deg or possibly lower and a skew angle of approximately 60 deg produces the best overall increase in skin friction. An increase in skin friction is desirable in this context as it implies a thinning of the boundary layer and, hence, a delay in the onset of separation. It appears that increasing the relative jet velocity increases the strength of the resulting vortices and that although this does enhance the desired effects, it also results in the vortices moving away from the surface more rapidly when in a counter-rotating configuration. It was also found that the jet slot aspect ratio had little effect on the resulting vortices, providing the jet mass flow rate remains the same. In all these respects, and in the rate at which vortex strength decays with distance downstream of the jet exits, the results accord with published experiments.

Much work remains to be done on defining the optimum values for the various parameters of the problem and on clarifying the actual mechanisms responsible for the establishment of the vortex. There is considerable scope for extending the studies of the interaction of the vortices and boundary layer in adverse pressure gradients and the consequent delay in boundary-layer separation which is one of the main thrusts of this work.

Acknowledgments

The authors gratefully acknowledge the support of British Aerospace Ltd. The authors would also like to thank C. M. Milford of British Aerospace, Military Aircraft, for many helpful discussions. CFDS-FLOW3D and Jasper are proprietary codes of CFDS, AEA Industrial Technology, Harwell, U.K.

References

[1]Taylor, H. D., "United Aircraft Research Department Summary Report on Vortex Generators," R-05280-9, 1950.

[2]Wallis, R. A., "A Preliminary Note on a Modified Type of Air-Jet for Boundary-Layer Control," ARC, Current-Paper CP 513, 1956.

[3]Pearcey, H. H., "Shock Induced Separation and Its Prevention," *Boundary Layer & Flow Control*, Vol. 2, Pergamon, New York, 1961, pp. 1170–1344.

[4]Johnston, J. P., and Nishi, M., "Vortex Generator Jets—A Means for Flow Separation Control," *AIAA Journal*, Vol. 28, No. 6, 1990, pp. 989–994.

[5]Compton, D. A., and Johnston, J. P., "Streamwise Vortex Production by Pitched and Skewed Jets in a Turbulent Boundary Layer," AIAA Paper 91-0038, 1991.

[6]Selby, G. V., Lin, J. C., and Howard, F. G., "Control of Low-speed Turbulent Separated Flow Using Jet Vortex Generators," *Experiments in Fluids*, Vol. 12, No. 6, 1992, pp. 394–400.

[7]Pearcey, H. H., Rao, K., and Sykes, D. M., "Inclined Air-jets used as Vortex Generators to Suppress Shock-induced Separation," AGARD Fluid Dynamics Symposium Computational and Experimental Assessment of Jets in Cross Flow, Winchester, U.K., April 1993.

[8]Anon., "FLOW3D Release 2.4: User Manual," CFDS, AEA Industrial Technology Harwell Lab., Oxfordshire, U.K., Nov. 1991.

[9]Henry, F. S., and Reynolds, A. J., "An Analytical Solution to Two Gradient Diffusion Models of Turbulence," *Journal of Fluids Engineering*, Vol. 106, 1984, pp. 211–216.

[10]Bradshaw, P., "The Analogy Between Stream-line Curvature and Buoyancy in Turbulent Shear Flow," *Journal of Fluid Mechanics*, Vol. 36, 1969, pp. 177–191.
[11]Henry, F. S., and Collins, M. W., "Prediction of Flow Over Helically Ribbed Surfaces," *International Journal for Numerical Methods in Fluids*, Vol. 13, 1991, pp. 321–340.
[12]Anon., "Environment User Guide," CFDS, AEA Industrial Technology Harwell Lab., Oxfordshire, U.K., Nov. 1992.
[13]Zhang, X., "Interaction Between a Turbulent Boundary Layer and Elliptic and Rectangular Jets," 2nd International Symposium on Engineering Turbulence Modeling and Measurements, Florence, Italy, May 31–June 1993.
[14]Kim, S.-W., and Benson, T. J., "Calculation of a Circular Jet in Crossflow with a Multiple-time-scale Turbulence Model," *International Journal Heat and Mass Transfer*, Vol. 35, No. 10, 1992, pp. 2357–2365.
[15]Jones, J. P., "The Calculation of the Paths of Vortices from a System of Vortex Generators, and a Comparison with Experiment," A.R.C., C.P. 361, 1955.
[16]Compton, D. A., and Johnston, J. P., Personal communication, Thermosciences Div., Mechanical Engineering Dept., Stanford Univ., Stanford, CA, 1993.
[17]Robertson, J. M., *Hydrodynamics in Theory and Application*, Prentice-Hall, Englewood Cliffs, NJ, 1965.
[18]Holmes, A. E., Hickey, P. K., Murphy, W. R., and Hilton, D.A., "The Application of Sub-boundary Layer Vortex Generators to Reduce Canopy 'Mach Rumble' Interior Noise on the Gulfstream III," AIAA 25th Aerospace Sciences Meeting, AIAA Paper 87-0084, 1987.